The EMBO Journal (2006) 25, 4650–4662 | © 2006 European Molecular Biology Organization | All Rights Reserved 0261-4189/06
www.embojournal.org

THE EMBO JOURNAL

Failure to prolyl hydroxylate hypoxia-inducible factor α phenocopies VHL inactivation *in vivo*

William Y Kim[1], Michal Safran[1], Marshall RM Buckley[1], Benjamin L Ebert[1,2], Jonathan Glickman[3], Marcus Bosenberg[4], Meredith Regan[5] and William G Kaelin Jr[1,6,*]

[1]Department of Medical Oncology, Dana-Farber Cancer Institute and Brigham and Women's Hospital, Harvard Medical School, Boston, MA, USA, [2]Broad Institute of MIT and Harvard, Cambridge, MA, USA, [3]Department of Pathology, Brigham and Women's Hospital, Harvard Medical School, Boston, MA, USA, [4]Department of Pathology, University of Vermont, Burlington, VT, USA, [5]Department of Biostatistics and Computational Biology, Dana-Farber Cancer Institute, Boston, MA and Department of Medicine, Harvard Medical School, Boston, MA, USA and [6]Howard Hughes Medical Institute, Chevy Chase, MD, USA

Many functions have been assigned to the von Hippel-Lindau tumor suppressor gene product (pVHL), including targeting the alpha subunits of the heterodimeric transcription factor HIF (hypoxia-inducible factor) for destruction. The binding of pVHL to HIFα requires that HIFα be hydroxylated on one of two prolyl residues. We introduced HIF1α and HIF2α variants that cannot be hydroxylated on these sites into the ubiquitously expressed *ROSA26* locus along with a Lox-stop-Lox cassette that renders their expression Cre-dependent. Expression of the HIF2α variant in the skin and liver induced changes that were highly similar to those seen when pVHL is lost in these organs. Dual expression of the HIF1α and HIF2α variants in liver, however, more closely phenocopied the changes seen after pVHL inactivation than did the HIF2α variant alone. Moreover, gene expression profiling confirmed that the genes regulated by HIF1α and HIF2α in the liver are overlapping but non-identical. Therefore, the pathological changes caused by pVHL inactivation in skin and liver are due largely to dysregulation of HIF target genes.

The EMBO Journal (2006) **25,** 4650–4662. doi:10.1038/sj.emboj.7601300; Published online 14 September 2006
Subject Categories: molecular biology of disease
Keywords: hypoxia-inducible factor; prolyl hydroxylase; von Hippel-Lindau

Introduction

von Hippel-Lindau (VHL) disease is a hereditary cancer syndrome characterized by the development of various tumors including retinal and central nervous system (CNS) hemangioblastomas, pheochromocytomas, and clear cell renal carcinomas (Kim and Kaelin, 2004). VHL patients carry one wild-type *VHL* allele and one mutated *VHL* allele in their germline. Pathology develops when the wild-type allele is somatically inactivated in a susceptible cell. Mutation or hypermethylation of the *VHL* locus is also very common in sporadic renal cell carcinomas and sporadic CNS hemangioblastomas (Kim and Kaelin, 2004).

The *VHL* gene product, pVHL, is the substrate recognition module for an E3 ubiquitin ligase complex that contains elongin B, elongin C, Cul2, and Rbx1 (Kaelin, 2002). Cells lacking pVHL constitutively over-produce hypoxia-inducible mRNAs (Gnarra *et al*, 1996; Iliopoulos *et al*, 1996; Siemeister *et al*, 1996; Stratmann *et al*, 1997). Many of these mRNAs are controlled by a heterodimeric transcription factor called hypoxia-inducible factor (HIF), which consists of a labile alpha subunit and a stable beta subunit. Humans possess three alpha subunit genes (*HIF1α*, *HIF2α*, or *HIF3α*) and three *HIFβ* genes (also called the aryl hydrocarbon receptor nuclear translocator (ARNT)) (Semenza, 2003). pVHL binds directly to HIFα subunits and orchestrates their polyubiquitination, leading to their destruction by the proteasome (Kaelin, 2002). The binding of pVHL to HIF is governed by an oxygen-dependent, post-translational modification (prolyl hydroxylation) of HIFα subunits catalyzed by EGLN family members (also called PHDs or HPHs) (Kaelin, 2005; Schofield and Ratcliffe, 2005). Thus, HIFα subunits are normally degraded in the presence of oxygen but are stabilized under hypoxic conditions or in the setting of pVHL loss, leading to transactivation of HIF target genes.

Over 60 HIF target genes have been identified, many of which play critical roles in cellular and systemic responses to hypoxia (Semenza, 2003). Target genes such as *VEGF* and *PDGF-B* are implicated in angiogenesis and likely contribute to the hypervascularity observed in VHL-associated tumors through their actions on endothelial cells and pericytes, respectively. Another HIF target, *TGFα*, is a powerful renal epithelial cell mitogen and probably contributes to the development of both hemangioblastoma and renal cell carcinoma (Kim and Kaelin, 2004).

HIF1α and HIF2α are not wholly redundant. *HIF1α*$^{-/-}$ mice die in midgestation and exhibit severe blood vessel defects (Iyer *et al*, 1998). *HIF2α*$^{-/-}$ mice also exhibit embryonic or early postnatal lethality but as a consequence of catecholamine deficiency or lung maturation defects (Tian *et al*, 1998; Peng *et al*, 2000; Compernolle *et al*, 2002). In a recent study, embryonic stem (ES) cells in which an HIF2α cDNA was homozygously inserted into the *HIF1α* locus were more angiogenic and tumorigenic than their wild-type counterparts (Covello *et al*, 2005). Finally, HIF1α and HIF2α produce overlapping yet distinct gene expression profiles. For example, HIF1α appears to be more important than HIF2α with respect to the hypoxic induction of glycolytic genes and the proapoptotic gene *BNip3* (Hu *et al*, 2003; Raval *et al*, 2005; Wang *et al*, 2005).

*Corresponding author. Department of Medical Oncology, Dana-Farber Cancer Institute and Brigham and Women's Hospital, Harvard Medical School, 44 Binney Street, Mayer 457, Boston, MA 02115, USA.
Tel.: +1 617 632 3975; Fax: +1 617 632 4760;
E-mail: William_kaelin@dfci.harvard.edu

Received: 3 May 2006; accepted: 26 July 2006; published online: 14 September 2006

HIF2α appears to play a special role in $VHL^{-/-}$ renal carcinomas. First, $VHL^{-/-}$ renal carcinomas express both HIF1α and HIF2α or exclusively HIF2α (Maxwell *et al*, 1999). Second, an apparent switch from HIF1α to HIF2α expression occurs in preneoplastic lesions arising in human $VHL^{+/-}$ kidneys in association with increasing dysplasia and cellular atypia (Mandriota *et al*, 2002). Third, inhibition of HIF2α by shRNA is sufficient to suppress $VHL^{-/-}$ tumor growth *in vivo* (Kondo *et al*, 2003; Zimmer *et al*, 2004). Finally, the ability of pVHL to suppress tumor formation by $VHL^{-/-}$ cells can be overridden by an HIF2α variant that cannot be prolyl hydroxylated, but not by the corresponding HIF1α variant (Maranchie *et al*, 2002; Kondo *et al*, 2002, 2003; Raval *et al*, 2005).

Genotype–phenotype correlations in VHL disease suggest, however, that pVHL has functions in addition to regulating HIF. For example, pVHL mutants that retain the ability to bind and polyubiquitinate HIF have been linked to familial pheochromocytoma (so-called type 2C VHL disease) (Cockman *et al*, 2000; Hoffman *et al*, 2001). Moreover, pVHL mutants linked to type 2A VHL disease (high risk of hemangioblastoma and pheochromocytoma and low risk of renal cell carcinoma) are, like 2B mutants (high risk of all three tumors), defective with respect to polyubiquitinating HIF, suggesting that a second pVHL function modulates renal cancer risk in the setting of VHL disease. Finally, patients with Chuvash polycythemia, who are homozygous for a hypomorphic *VHL* allele, develop polycythemia (presumably due to a quantitative HIF defect leading to increased erythropoietin (EPO) production) but are not tumor prone (Ang *et al*, 2002; Pastore *et al*, 2003; Gordeuk *et al*, 2004).

Biochemical studies also suggest that pVHL has multiple functions. pVHL has been reported to polyubiquitinate atypical protein kinase C, two deubiquitinating enzymes (VHL-interacting deubiquitinating enzyme 1 and 2), and two subunits of RNA polymerase II (hsRBP7 and the hyperphosphorylated from of Rbp1) (Czyzyk-Krzeska and Meller, 2004). Furthermore, pVHL has been reported to bind directly to the plant homeodomain protein, Jade-1, and to the KRAB-A domain-containing protein, VHLaK (Czyzyk-Krzeska and Meller, 2004). Gene expression studies also support that pVHL has HIF-independent functions (Wykoff *et al*, 2000, 2004; Zatyka *et al*, 2002; Jiang *et al*, 2003).

The existence of HIF-independent pVHL functions might explain the observation that forced activation of HIF target genes in animal models has not caused tumors. Production of nondegradable forms of HIF or HIF-like proteins in mouse skin and rabbit musculature induces normal appearing blood vessels (Vincent *et al*, 2000; Elson *et al*, 2001). This might suggest that dysregulation of HIF is not sufficient to promote tumor formation. A caveat, however, is that these studies were conducted using HIF1α (or variants thereof) leaving open the possibility that increased HIF2α or HIF3α activity, alone or together with HIF1α, is required for tumor formation. It is also possible tumor promotion by HIF is context dependent with respect to tissue and species. This would explain the limited spectrum of tumors observed in VHL patients and the discordance between mice and man with respect to the tissues affected by pVHL loss.

$VHL^{-/-}$ mice die during embryogenesis due to placental insufficiency while $VHL^{+/-}$ mice develop cavernous liver hemangiomas (Gnarra *et al*, 1997; Haase *et al*, 2001; Ma *et al*, 2003). Similar liver abnormalities are observed with shorter latency and higher penetrance when pVHL is conditionally inactivated in hepatocytes of *VHL flox/flox* mice. In addition, such mice are runted, die prematurely, and develop steatosis (Haase *et al*, 2001; Ma *et al*, 2003). A recent study showed that these hepatic lesions could be prevented by simultaneous deletion of *ARNT* (but not by elimination *HIF1α*) implying that dysregulation of at least one ARNT partner other than HIF1α is *necessary* for the development of these lesions (Rankin *et al*, 2005). In this report, we show that dysregulation of HIF2α is *sufficient* to partially phenocopy pVHL loss in the skin and liver and that simultaneous dysregulation of HIF1α and HIF2α in the liver produces lesions that are virtually indistinguishable from those observed after pVHL inactivation in that organ.

Results

Generation of mouse strains that conditionally produce HIF1α or HIF2α variants

We set out to make mice in which hemagglutinin (HA)-tagged HIF1α or HIF2α variants that escape recognition by pVHL due to proline to alanine substitutions (hereafter called HIF1dPA and HIF2dPA for simplicity) could be conditionally expressed in tissues of interest. Earlier studies showed that these variants are relatively stable compared to their wild-type counterparts and retain the ability to transcriptionally activate HIF target genes (Masson *et al*, 2001; Hu *et al*, 2003; Kondo *et al*, 2003). In this way, we hoped to ask whether activation of HIF target genes is sufficient to induce pathological changes observed when pVHL function is compromised.

Toward this end we created targeting vectors for inserting the HIF1dPA or HIF2dPA cDNA into the mouse *ROSA26* locus by homologous recombination (Figure 1A). Both targeting vectors also introduced a Lox-stop-Lox cassette 5′ of the cDNAs so that their transcription would be dependent upon Cre-mediated excision of the stop element (Jackson *et al*, 2001; Mao *et al*, 2001; Srinivas *et al*, 2001). The *ROSA26* locus is dispensible for normal development and heterologous genes placed under its control are ubiquitously expressed (Zambrowicz *et al*, 1997; Soriano, 1999; Mao *et al*, 2001; Srinivas *et al*, 2001). ES cells that had undergone homologous recombination with the targeting constructs for ROSA26-HA-HIF1dPA and ROSA26-HA-HIF2dPA, as determined by Southern blot analysis (Figure 1B) and PCR (data not shown), were microinjected into C57/B6 blastocysts to generate chimeric mice. Germline transmission was confirmed by detection of the targeted *ROSA26* locus in the offspring of chimeras (data not shown).

In pilot experiments, mouse embryo fibroblasts (MEFs) were isolated from embryos of *HIF1dPA/+* and *HIF2dPA/+*, or wild-type littermate controls and infected with adenovirus encoding Cre recombinase. Exposure to Cre led to successful recombination of the targeted allele (Figure 1C). As expected, HA-HIF1α and HA-HIF2α were detectable in lysates derived from *HIF1dPA/+* and *HIF2dPA/+* MEFs infected with adenoviral-Cre, but not in wild-type littermate control MEFs infected with adenoviral-Cre. HA-HIF1α and HA-HIF2α were not detectable in uninfected MEFs (Figure 1D). The levels of HA-HIF1α were lower than that of HA-HIF2α, possibly due to the existence of pVHL-independent ubiquitin ligases that can target HIF1α (Ravi *et al*, 2000; Isaacs *et al*, 2002). In support

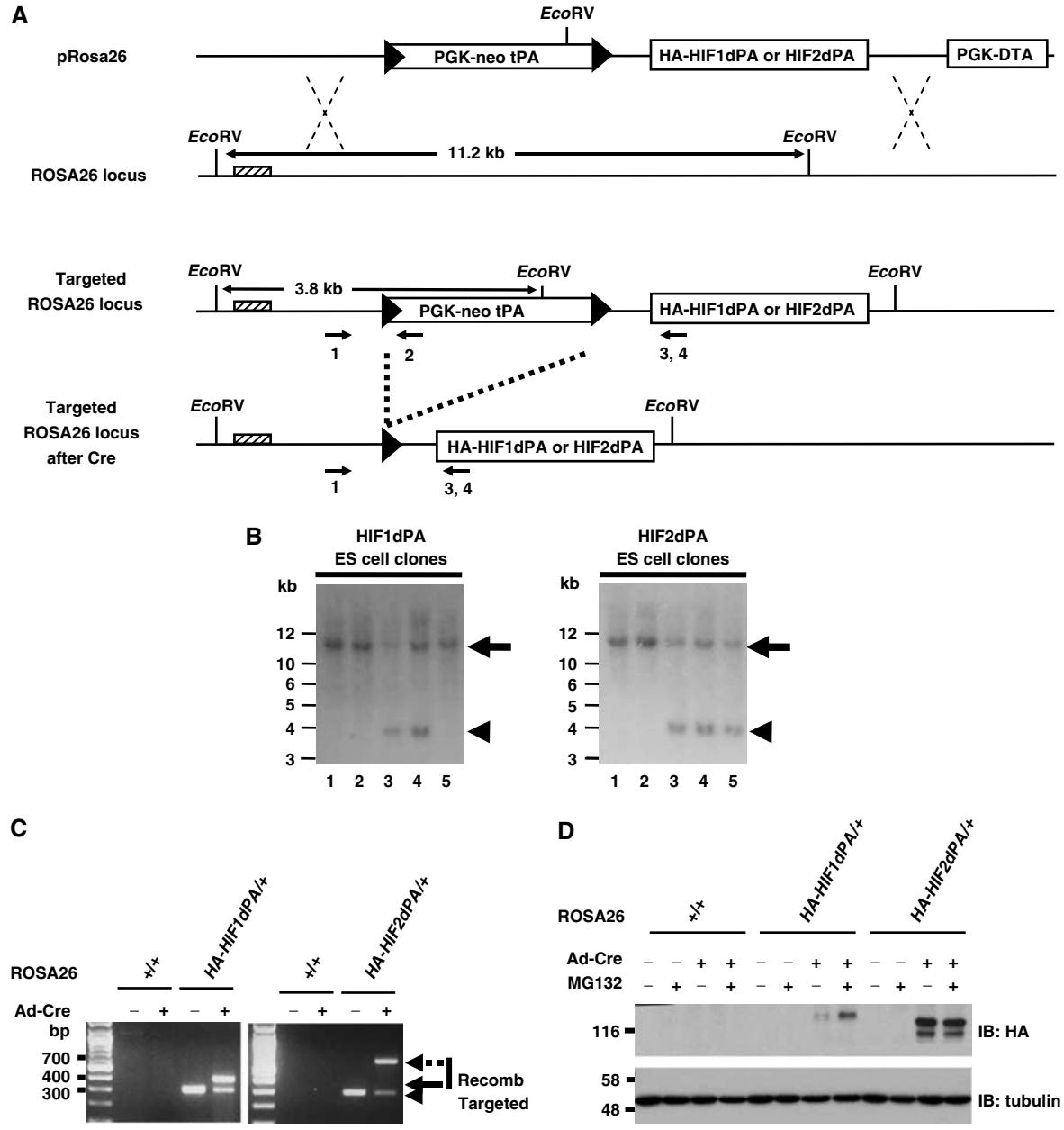

Figure 1 Insertion of HA-HIF1dPA and HA-HIF2dPA cassettes into ROSA26 locus by homologous recombination. (**A**) Schematic of the pRosa26-HA-HIF1dPA and pRosa26-HA-HIF2dPA targeting vectors and the Rosa26 locus before and after Cre-mediated excision of the transcriptional stop element. LoxP sites are represented by the arrowheads and the 5′ external probe is indicated by the hatched rectangle. Shown also are the primers (arrows) used for the generation of (C). (**B**) Representative Southern blots of individual ES clones after electroporation with indicated targeting vectors and drug selection. Genomic DNA was digested with *Eco*RV and hybridized to 5′ external probe. The wild-type locus produces an 11.2 kb fragment (arrow). Successful recombination is indicated by the presence of a 3.8 kb fragment (arrowhead), which arises because of an internal *Eco*RV site in the stop element. (**C**) MEFs were infected with an adenovirus expressing Cre recombinase. DNA was extracted from the MEFs 48 h later and PCR was performed using primers (see (A)) that differentiate the targeted allele (300 bp product; arrowhead) (primers 1 and 2) from the recombined alleles (400 bp product for HIF1dPA; arrow) (primers 1 and 3) and 700 bp product for HIF2dPA; dashed arrow (primers 1 and 4)). (**D**) MEFs with the indicated genotypes were infected with adenoviral Cre. The proteasome inhibitor MG132 (+) or DMSO (−) was added 48 h later. Immunoblot analysis was performed 6 h later with the indicated antibodies.

of this idea, HA-HIF1α, but not HA-HIF2α, was sensitive to the addition of the proteasome inhibitor MG132 (Figure 1D). Likewise, the abundance of endogenous HIF1α, but not HIF2α, increased after treatment of VHL−/− human renal carcinoma cells with MG132, indicating that the behavior of HA-HIF1α was not peculiar to the transgene (Figure 2A).

The levels of HA-HIF1α and HA-HIF2α achieved after Cre-mediated activation in *HIFdPA/+* MEFs were comparable to the levels of their endogenous murine counterparts in *VHL−/−* MEFs, as determined by immunoblot analysis with antibodies against epitopes that are conserved between human and mouse HIF1α or human and mouse HIF2α, respectively (Figure 2B). Similar results were obtained with two independent antibodies for each HIFα protein (data not shown). The levels of HA-HIF1α and HA-HIF2α were somewhat lower than observed in VHL−/− human renal carcinoma

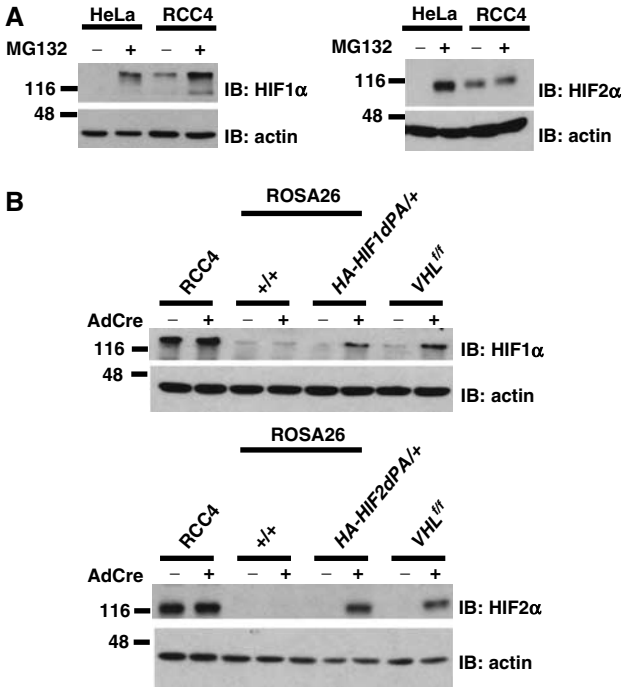

Figure 2 Expression levels of HA-HIF1α and HA-HIF2α. (**A**) Immunoblot analysis of HeLa and RCC4 cells treated with the proteasome inhibitor MG132 (+) or DMSO (−) for 6 h. (**B**) Immunoblot analysis of RCC4 cells or MEFs with the indicated genotypes. Where indicated, cells were infected with an adenovirus encoding Cre recombinase 72 h before lysis.

cells (Figure 2B). Although the significance of this finding is not clear, it suggests that the results described below are not due to gross overexpression of the HIFα transgenes. The levels of HA-HIF1α and HA-HIF2α achieved following Cre exposure were associated with induction of known HIF target genes, such as *VEGF, ADRP, Egl nine homolog 3 (EglN3)* and *Glut1* (Supplementary Figure 1A and B).

HIF2α causes skin changes that are similar to those observed after pVHL loss

To test whether the conditional alleles were functional *in vivo*, we next crossed the HIF1dPA and HIF2dPA mice to mice (*K14-Cre*) expressing Cre recombinase under the control of the keratin14 promoter. In parallel, we crossed mice carrying a conditional *VHL* allele ($VHL^{flox/flox}$, hereafter referred to as $VHL^{f/f}$ for simplicity) (Haase *et al*, 2001) to *K14-Cre* mice. The *K14-Cre* transgene efficiently deletes LoxP containing alleles in the basal keratinocytes of the epidermis (Indra *et al*, 2000). Earlier transgenic experiments indicated that overproduction of specific isoforms of the HIF target gene *VEGF* in keratinocytes induces the formation of leaky blood vessels and skin ulceration (Larcher *et al*, 1998; Thurston *et al*, 1999), while overproduction of a stabilized HIF1α deletion mutant leads to the robust induction of normal appearing blood vessels (Elson *et al*, 2001).

HA-HIF1α and HA-HIF2α were, as expected, detected specifically in extracts prepared from skin of *K14-Cre;HIF1dPA* and *K14-Cre;HIF2dPA* mice, respectively (Figure 3A). However, HIF1dPA levels were much lower than HIF2dPA, which is similar to the results obtained with MEFs (Figure 1D). By postnatal day 5 the skin of *K14-Cre;HIF2dPA* and *K14-Cre;*$VHL^{f/f}$ mice was noticeably red and could easily be distinguished from the skin of littermate controls (data not shown). By weaning age, the mice exhibited skin erythema, partial alopecia, and runting (Figure 3B and C). These phenotypes were only observed in animals that carried both the *K14-Cre* transgene and either the *HIF2dPA* allele or homozygous *VHL floxed* alleles. We did not observe a gross skin phenotype in the *K14-Cre;HIF1dPA* mice (data not shown). This might reflect the lower levels of HIF1α achieved in this system relative to HIF2α (Figure 3A).

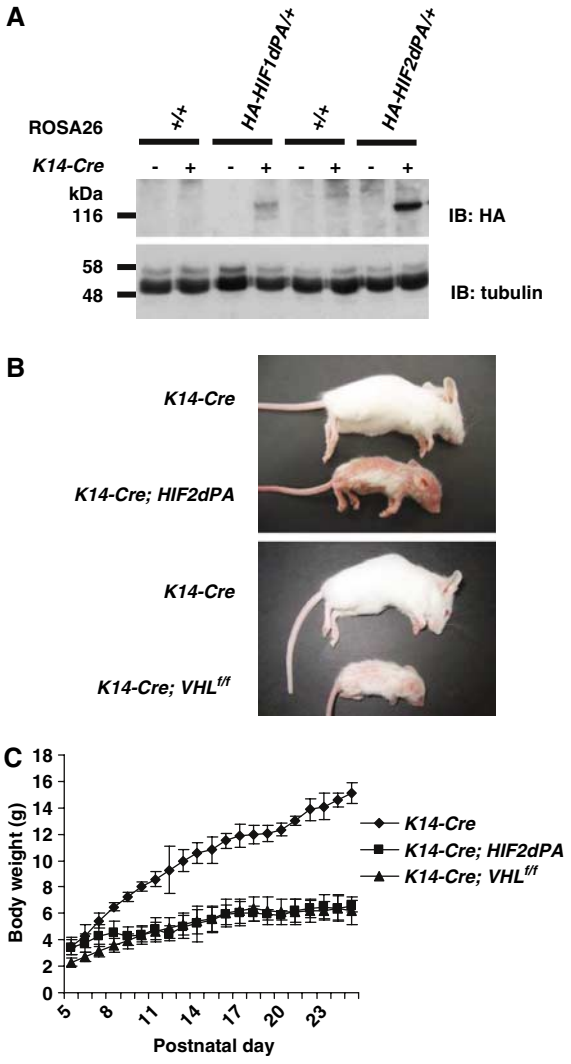

Figure 3 Gross phenotypes of *K14-Cre;HIF2dPA* mice and *K14-Cre;*$VHL^{f/f}$ mice. (**A**) Immunoblot analysis of skin biopsy homogenates prepared from mice with the indicated genotypes. (**B**) Photographs of representative *K14-Cre;HIF2dPA* and *K14-Cre;*$VHL^{f/f}$ mice alongside age and sex-matched *K14-Cre* control. (**C**) Growth curves of mean body weight of *K14-Cre;HIF2dPA*, *K14-Cre;*$VHL^{f/f}$ mice, and *K14-Cre* mice.

HIF2α, like pVHL loss, induces the formation of nonleaky blood vessels and epidermal hyperproliferation

H&E staining of furred and unfurred skin from both *K14-Cre;HIF2dPA* and *K14-Cre;*$VHL^{f/f}$ mice showed epidermal hyperplasia and an increased number of dilated dermal blood vessels (Figure 4A). CD31 staining confirmed an increase in vascular density of the skin from *K14-Cre;HIF2dPA*

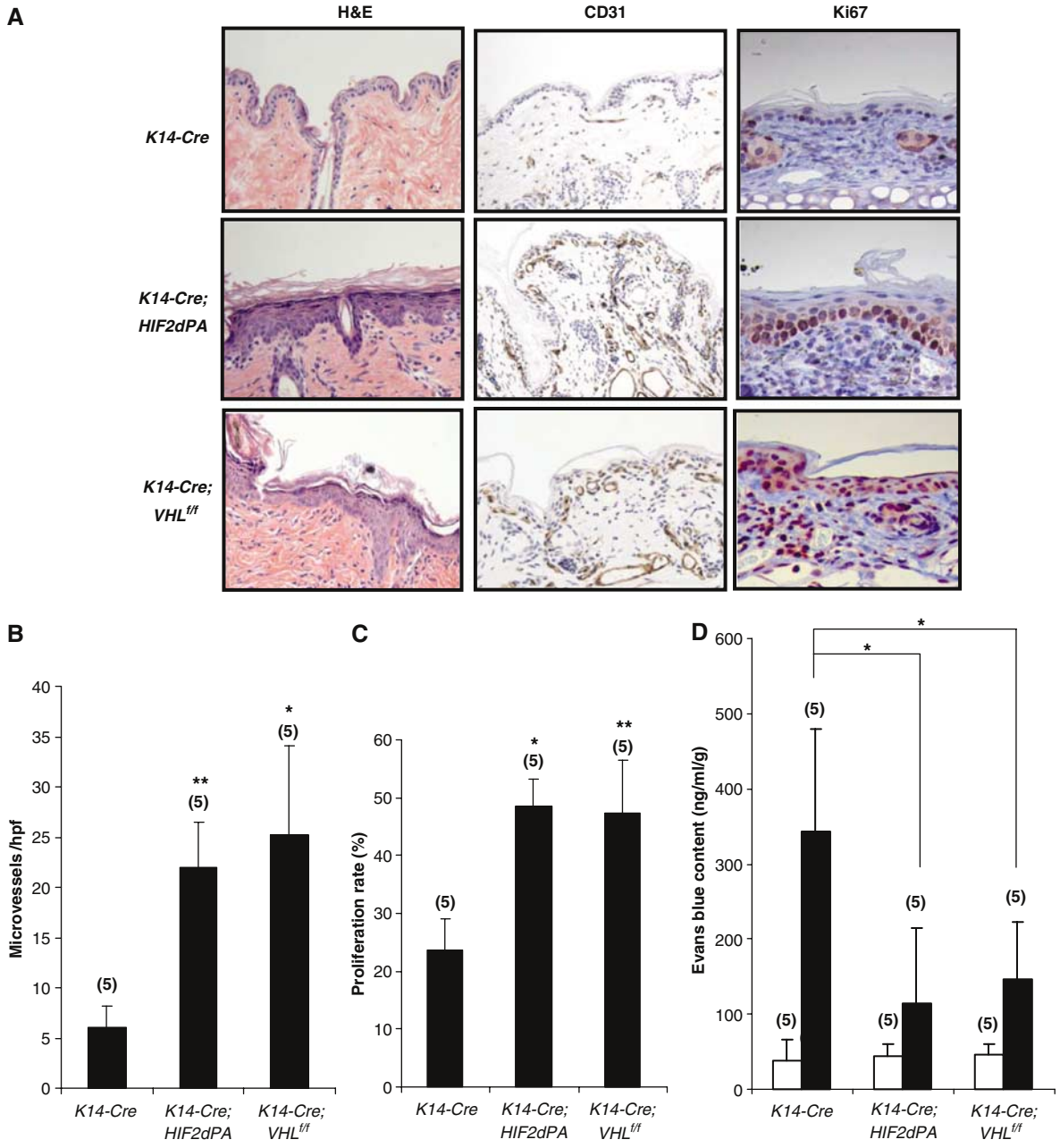

Figure 4 Histological and functional changes in the skin and vasculature of *K14-Cre;HIF2dPA* and *K14-Cre;VHL$^{f/f}$* mice. (**A**) Representative histological sections of skin from 6- to 8-week-old mice with the indicated genotypes after staining with hematoxylin and eosin (H&E) (× 100) or with antibodies against CD31 (× 100) or Ki67 (× 400). CD31 and Ki67 sections were counterstained with hematoxylin. (**B**) Quantitation of microvessel density. Error bars = 1 s.d. (*$P<0.05$, **$P<0.01$). (**C**) Quantitation of Ki67 + cells. Error bars = 1 s.d. (*$P<0.05$, **$P<0.01$). (**D**) Evans blue vascular permeability assay comparing mean dye extravasation at baseline (white) and after topical application of mustard oil (black). Error bars = 1 s.d. (*$P<0.05$).

and *K14-Cre;VHL$^{f/f}$* mice (particularly notable at the dermal–epidermal junction) and the appearance of ectatic vessels deeper within the dermis ($P<0.01$ and <0.05, respectively) (Figure 4A and B). Both *K14-Cre;HIF2dPA* and *K14-Cre;VHL$^{f/f}$* mice displayed an increase in Ki67 staining of keratinocytes relative to *K14-Cre* mice, indicative of increased keratinocyte proliferation ($P<0.05$ and <0.01 respectively) (Figure 4C).

To better understand the effects of HIF2α stabilization and pVHL loss on the function of the dermal vasculature, we performed Evans blue vascular permeability assays on *K14-Cre;HIF2dPA* and *K14-Cre;VHL$^{f/f}$* mice. Baseline vascular leakage of both *K14-Cre;HIF2dPA* and *K14-Cre;VHL$^{f/f}$* mice was similar to that of *K14-Cre* mice following Evans blue dye injection (Figure 4D). After application of mustard oil (an inflammatory stimulus) both *K14-Cre;HIF2dPA* and *K14-Cre;VHL$^{f/f}$* mice showed a *decreased* level of blood vessel leakage compared to *K14-Cre* controls ($P<0.05$) (Figure 4D), consistent with an earlier study in which a nondegradable version of HIF1α was expressed under the control of the K14 promoter (Elson *et al*, 2001). Therefore, the skin vessels that form as a consequence of HIF2α activation or pVHL loss in keratinocytes are not conspicuously leaky.

Gross liver changes induced by HIF activation in hepatocytes

Having established that the *HIF1dPA* and *HIF2dPA* alleles could be successfully recombined with Cre *in vivo*, and that HIF2α dysregulation could phenocopy pVHL loss in the skin, we next turned our attention to the liver because earlier work showed that *VHL* inactivation in this organ, either stochastically (in $VHL^{+/-}$ mice) or conditionally (in $VHL^{f/f}$ mice) in mice, leads to hepatomegaly, steatosis, and blood vessel proliferation, including hemangioma-like lesions (Haase *et al*, 2001; Ma *et al*, 2003).

To this end, we crossed the transgenic mice expressing Cre recombinase under the control of a hepatocyte-specific promoter (*Alb-Cre*) with the *HIF1dPA* mice, *HIF2dPA* mice, and $VHL^{f/f}$ mice. The *Alb-Cre* transgene efficiently deletes loxP containing alleles in hepatocytes of mouse livers (Postic *et al*, 1999). The hepatic HA-HIF1dPA levels in *Alb-Cre;HIF1dPA* mice were much lower than the hepatic HA-HIF2dPA levels in *Alb-Cre;HIF2dPA* mice (Figure 5A), consistent with the differences we observed in MEFs (Figure 1D) and skin (Figure 3A).

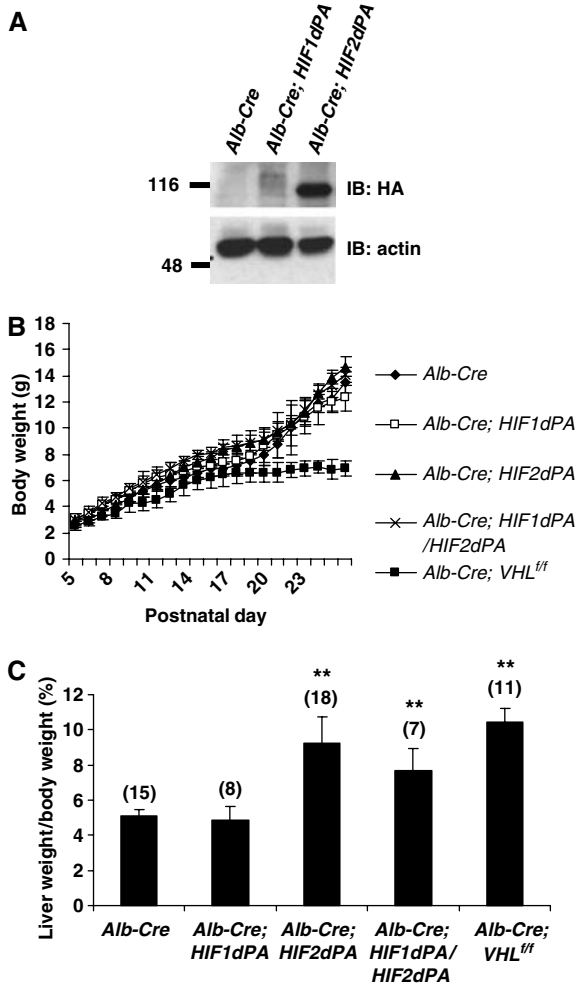

Figure 5 Body weight and liver weight changes induced by pVHL loss or HIF2 activation. (**A**) Immunoblot analysis of liver homogenates prepared from mice with the indicated genotypes. (**B**) Growth curves of mean body weight of mice with the indicated genotypes. (**C**) Mean liver weights (as a percentage of body weight) of 6- to 8-week-old mice with the indicated genotypes. Error bars = 1 s.d. (**$P<0.01$).

As expected, $Alb\text{-}Cre;VHL^{f/f}$ mice were runted relative to littermate controls (Figure 5B) and died at approximately 6–8 weeks of age (data not shown). Interestingly, *Alb-Cre;HIF2dPA* and *Alb-Cre;HIF1dPA/HIF2dPA* mice also died at 6–8 weeks of age but maintained a normal body weight (Figure 5B and data not shown). In contrast, *Alb-Cre;HIF1dPA* mice were indistinguishable from littermate controls and did not appear to have a shortened lifespan.

$Alb\text{-}Cre;VHL^{f/f}$, *Alb-Cre;HIF2dPA*, and *Alb-Cre;HIF1dPA/HIF2dPA* mice all had marked hepatomegaly with liver weights (as a percentage of body weight) approximately twice that of controls (each $P<0.01$) when killed at 6 weeks of age (Figure 5C). $Alb\text{-}Cre;VHL^{f/f}$ and *Alb-Cre;HIF1dPA/HIF2dPA* livers were indistinguishable from one another on gross inspection and clearly abnormal. They were friable and appeared stippled with irregular, yellow spots (suggestive of steatosis) on a reddish background (Figure 6). *Alb-Cre;HIF2dPA* livers were also easy to visually discriminate from controls by their homogeneous deep maroon color. *Alb-Cre;HIF1dPA* livers were similar in weight and appearance to control livers (Figures 5C and 6).

Simultaneous activation of HIF1α and HIF2α in hepatocytes is sufficient to induce histological changes observed after pVHL inactivation in the liver

The livers of $Alb\text{-}Cre;VHL^{f/f}$ and *Alb-Cre;HIF1dPA/HIF2dPA* mice were virtually indistinguishable when stained with H&E and examined histologically. Both showed collections of irregular, dilated, blood filled sinusoids and cytoplasmic vacuolization in hepatocytes with eccentric nuclei (suggestive of steatois) (Figure 6). H&E stains of *Alb-Cre;HIF2dPA* livers demonstrated similar vascular lesions but with minimal evidence of vacuolization (Figure 6). *Alb-Cre;HIF1dPA* livers had a fine vacuolization of hepatocytes but were otherwise similar to controls. Staining with CD34 and quantitation of microvascular density confirmed the apparent increase in vascularity in *Alb-Cre;HIF2dPA*, *Alb-Cre;HIF1dPA/HIF2dPA*, and $Alb\text{-}Cre;VHL^{f/f}$ livers relative to controls ($P<0.01$, <0.01, and <0.5, respectively) (Figure 7A and B).

Consistent with their macroscopic and H&E appearance, $Alb\text{-}Cre;VHL^{f/f}$ and *Alb-Cre;HIF1dPA/HIF2dPA* livers had a clear increase in lipid accumulation within hepatocytes in a mixed micro and macrovesicular steatotic pattern, as determined by Oil Red O staining, whereas *Alb-Cre;HIF1dPA* livers showed moderate lipid accumulation in a microvesicular pattern (Figure 7A). *Alb-Cre;HIF2dPA* livers had minimal lipid accumulation over controls.

Ki67 staining of *Alb-Cre;HIF2dPA, Alb-Cre;HIF1dPA/HIF2dPA,* and $Alb\text{-}Cre;VHL^{f/f}$ and livers revealed a clear increase in Ki67 staining of hepatocytes indicative of increased proliferation relative to littermate controls ($P<0.01$, <0.01, and <0.001, respectively) (Figure 7A and C). A number of different cell types exhibited Ki67 positivity including hepatocytes and uncharacterized cells located within the hepatic sinusoids. The proliferation rate of *Alb-Cre;HIF1dPA* hepatocytes was normal.

Hematological effects of HIF activation or pVHL loss in the liver

The liver is capable of producing EPO and $Alb\text{-}Cre;VHL^{f/f}$ mice have been reported to develop polycythemia secondary

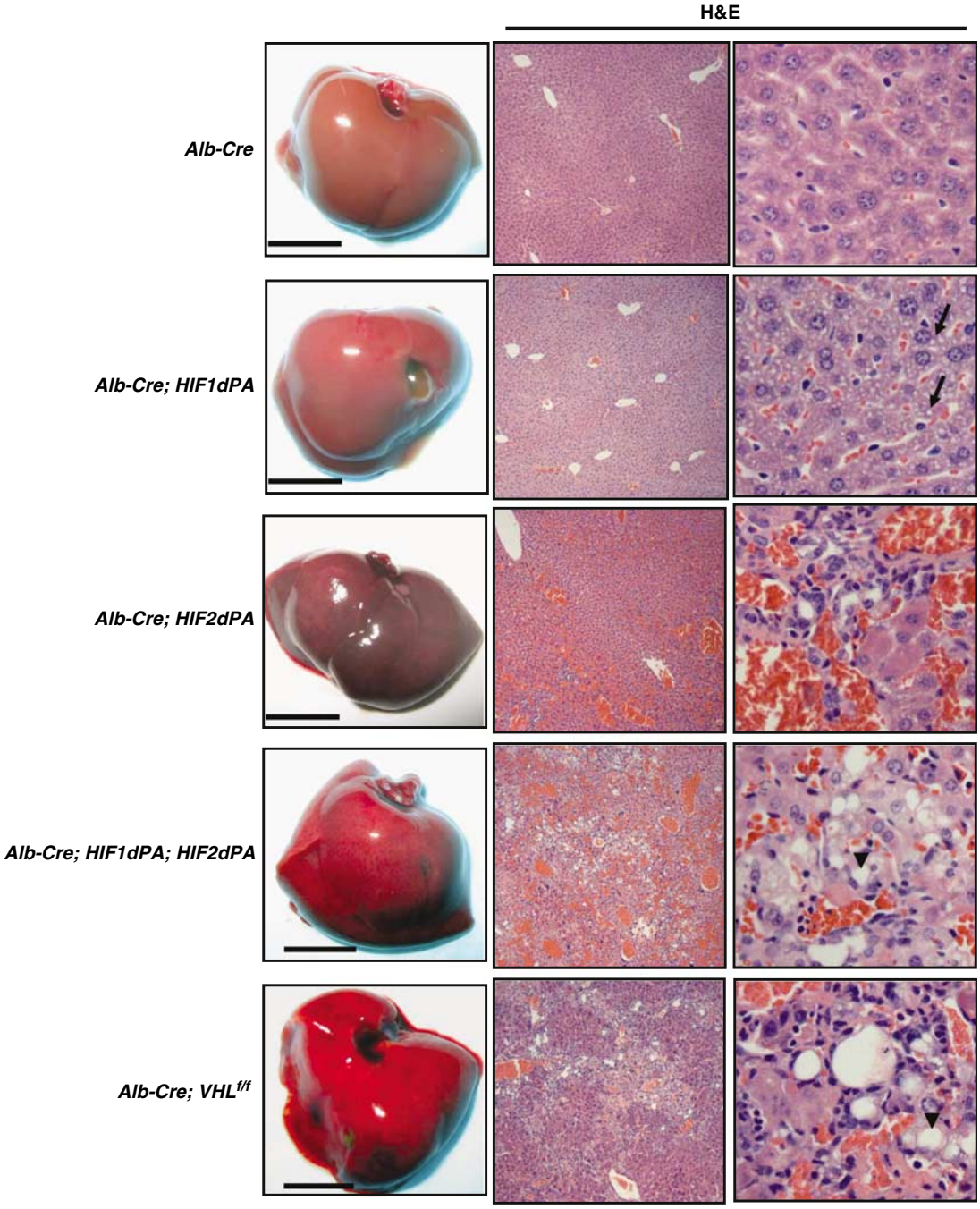

Figure 6 Gross and histological hepatic changes induced by pVHL loss or HIF activation. Representative photographs of livers from 6- to 8-week-old mice with the indicated genotypes (left column) along with histological sections after staining with H&E at × 100 (middle column) and × 400 (right column). Arrowheads indicate macrovesicular steatosis, arrows indicate microvesicular steatosis.

to elevated levels of this hormone (Haase *et al*, 2001). In our experiments, *Alb-Cre;HIF2dPA*, *Alb-Cre;HIF1dPA/HIF2dPA*, and *Alb-Cre;VHL*$^{f/f}$ mice all displayed noticeable erythema of the paws and unfurred skin by 4–6 weeks of age (data not shown). We postulated this was secondary to polycythemia. Indeed, hematocrit, reticulocyte, and EPO levels were all elevated in *Alb-Cre;HIF2dPA*, *Alb-Cre;HIF1dPA/HIF2dPA*, and *Alb-Cre;VHL*$^{f/f}$ mice relative to controls and *Alb-Cre;HIF1dPA* mice (Figure 8A–C). The increased EPO levels observed after pVHL inactivation relative to HIF2α activation (with or without HIF1α activation) was of borderline statistical significance because of the large variance within the *VHL*$^{f/f}$ group. Polycythemia might have contributed to the earlier deaths of these animals.

Gene expression changes after HIF activation or pVHL loss in the liver

The livers of mice in which HIF1α and HIF2α were simultaneously activated appeared strikingly similar to those in which pVHL had been lost. We next employed oligonucleotide microarrays to compare gene expression in the livers producing HIF1dPA, HIF2dPA, both HIF1dPA and HIF2dPA, or lacking pVHL. We first identified the top 200 genes that are upregulated in the *Alb-Cre;VHL*$^{f/f}$ mice compared to *Alb-Cre*

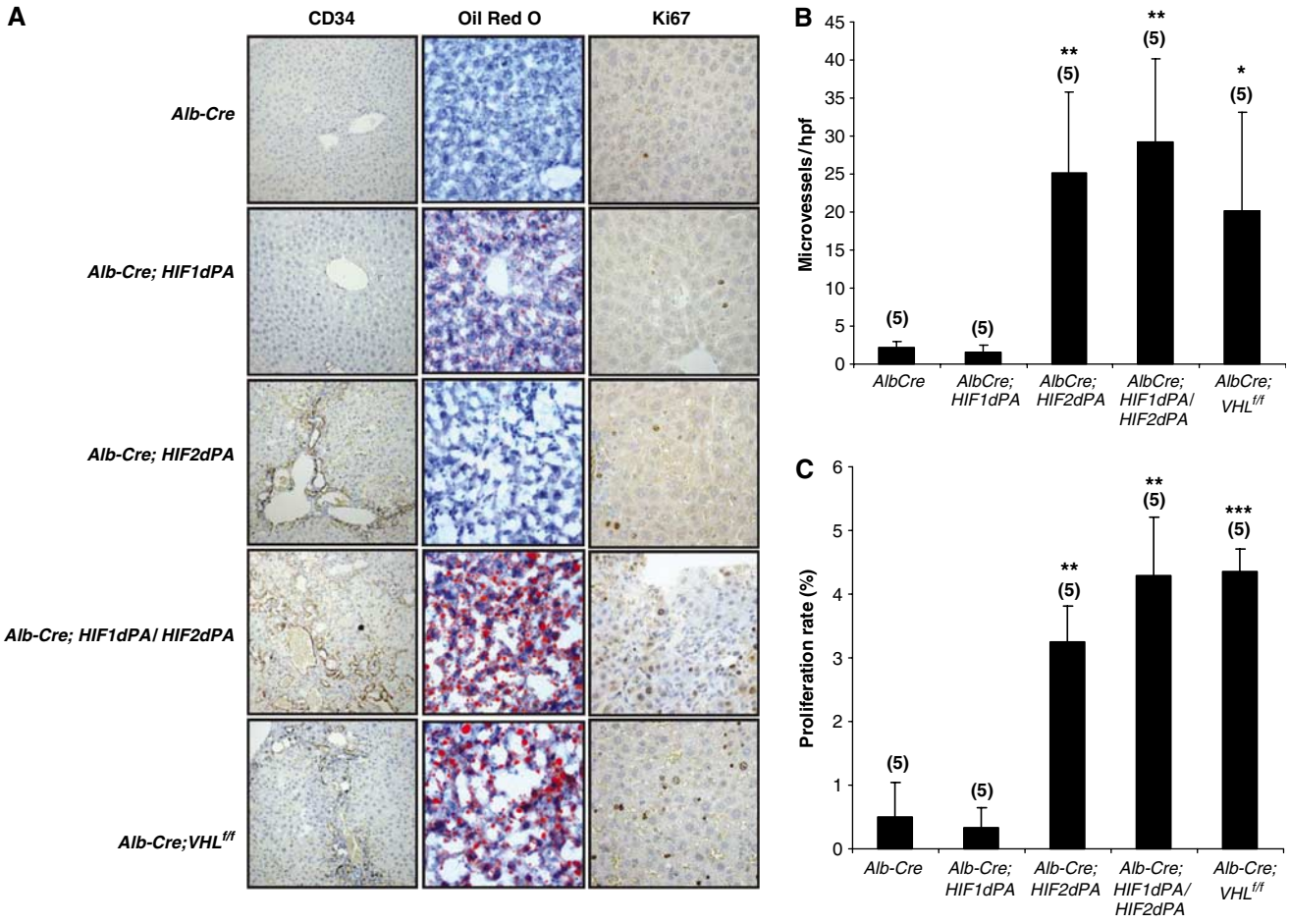

Figure 7 Hepatic changes in vascularity, fat accumulation, and proliferation induced by pVHL loss or HIF activation. (**A**) Histological sections of livers obtained from 6- to 8-week-old mice with the indicated genotypes after staining for antibodies against CD34 (× 100) or Ki67 (× 200) or with Oil Red O (× 200). (**B**) Quantitation of microvessel density. Error bars = 1 s.d. (*$P<0.05$; **$P<0.01$). (**C**) Quantitation of Ki67+ cells. Error bars = 1 s.d. (**$P<0.01$; ***$P<0.001$).

control mice, all of which were significant at $P<0.01$ by permutation testing. Using gene set enrichment analysis (GSEA) (Subramanian *et al*, 2005), we asked whether activation of HIF1α, HIF2α, or both could induce the signature of pVHL inactivation. All genes on the microarray were ranked by signal-to-noise ratio (Golub *et al*, 1999) as compared to the *Alb-Cre* control. The enrichment score was derived from the position of the genes in the VHL signature in these ranked lists. Activation of HIF1α in hepatocytes led to an enrichment score of 0.71 ($P=0.056$), indicating that the similarity between the genes regulated by HIF1α and VHL in this system approaches but does not reach statistical significance (Figure 9A). In contrast, activation of HIF2α or simultaneous activation of both HIF1α and HIF2α resulted in highly statistically significant enrichment scores of 0.93 and 0.91, respectively (both $P<0.001$) (Figure 9A). Hence, the vast majority of genes upregulated upon pVHL loss are also induced by HIF2α (with or without HIF1α activation).

The presence of microvesicular steatosis in the livers of mice expressing the activated form of HIF1α strongly suggested that some genes were specifically regulated by HIF1α and not HIF2α. This existence of such genes was confirmed in the microarray analysis (Figure 9B). For example, certain glycolytic genes such as *enolase 1*, *pyruvate kinase L*, and *aldolase C* were selectively activated by HIF1α, in keeping with earlier work in other models (Hu *et al*, 2003; Raval *et al*, 2005; Wang *et al*, 2005) while other known HIF target genes such as *PAI-1*, *annexin V*, and *EglN3* (Aprelikova *et al*, 2004; Schofield and Ratcliffe, 2004) were specifically upregulated by HIF2α (Figure 9B and Supplementary data). Therefore, in this model, HIF1α and HIF2α regulate an overlapping but distinct set of genes.

Discussion

We found that production of an HIF2α variant (HIF2dPA) that escapes recognition by pVHL in keratinocytes of genetically engineered mice is sufficient to phenocopy the runting, epidermal hyperplasia, and hypervascularity seen when pVHL is lost in this cellular compartment. Interestingly, production of this HIF2α variant within hepatocytes is sufficient to recapitulate the vascular lesions seen when pVHL is inactivated in liver parenchyma, while production of the corresponding HIF1α variant (HIF1dPA) causes microvesicular steatosis. Simultaneous expression of both HIFα variants in hepatocytes causes pathological changes, including increased vascularity and macrovesicular steatosis, that are indistinguishable from those seen when pVHL is lost in

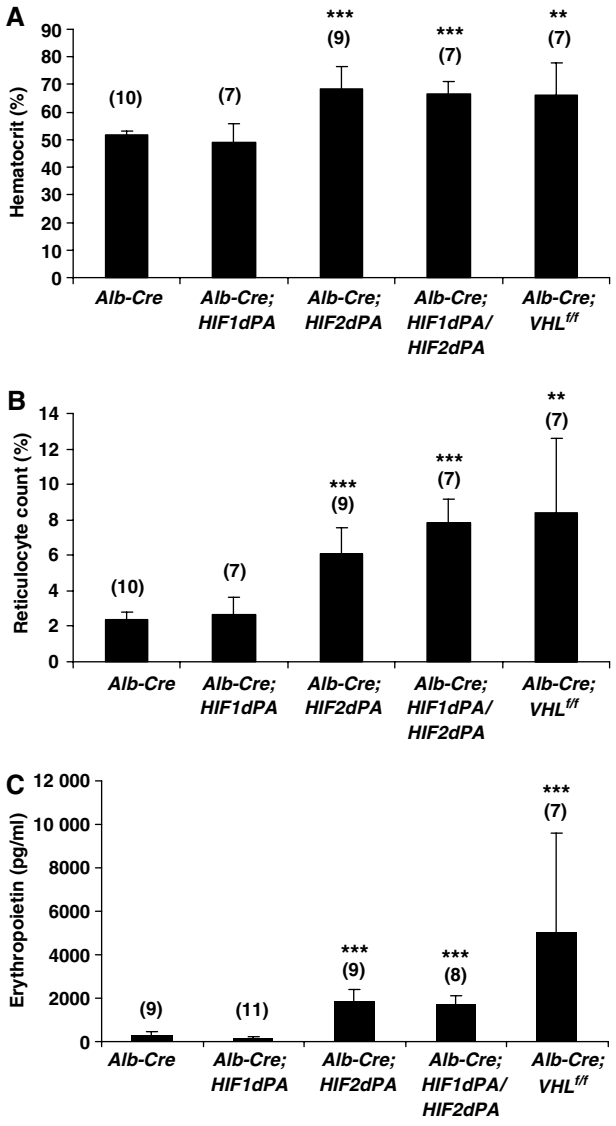

Figure 8 Hematological changes induced by pVHL loss or HIF activation. Mean hematocrits (**A**), reticulocyte counts (**B**), and serum EPO levels (**C**) from 6- to 8-week-old mice with the indicated genotypes. Error bars = 1 s.d. (**$P<0.01$; ***$P<0.001$).

these cells. Additionally, activation of HIF2α (with or without HIF1α) induces the gene expression signature of pVHL loss. Collectively these results suggest that the pathological changes seen after pVHL inactivation in skin and liver are primarily due to dysregulation of HIF target genes. Moreover, both the histological changes and the microarray analyses suggest that HIF1α and HIF2α are not wholly redundant with respect to these hepatic changes but instead cooperate with one another.

The experiments described were designed to compare the consequences of pVHL loss to HIFα activation and some of the differences observed between HIF1α and HIF2α should be interpreted cautiously. HIF1dPA and HIF2dPA were both under the control of a foreign promoter (ROSA26) and both lacked their native 5′ and 3′UTRs. It is also possible that the functional (e.g., DNA-binding and transactivation) assays performed so far are not sensitive enough to detect biologically relevant changes, beyond changes in protein stability, induced by the proline to alanine substitutions. The ability of HIF1dPA to induce certain genes and phenotypes, however, despite its lower levels relative to HIF2dPA, argues strongly that such genes and phenotypes are indeed preferentially regulated by HIF1α. On the other hand, failure of HIF1dPA to induce certain genes and phenotypes could be due to the technical considerations outlined above.

For example, we did not observe a skin phenotype in mice expressing HIF1dPA in keratinocytes under control of the ROSA26 promoter. This is in contrast to Arbeit and coworkers who observed the induction of normal appearing blood vessels in transgenic mice expressing this same mutant (Jeff Arbeit, personal communication), or an HIF1α variant lacking the oxygen-dependent degradation domain (Elson *et al*, 2001), under the control of the K14 promoter. This discrepancy might be due to technical differences, such as differences in the strengths of the ROSA26 and K14 promoters. We did, however, observe changes similar to those reported by Elson and co-workers when HIF2dPA was expressed in keratinocytes, probably due to the higher levels of HIF2dPA we achieved in our mice relative to HIF1dPA. This would argue that either HIF1α or HIF2α is capable of inducing skin blood vessel formation. Expression of HIF2dPA or inactivation of pVHL in the mouse epidermis also causes systemic weight loss. A similar phenotype after pVHL inactivation in the skin has been observed by Randy Johnson (R Johnson, personal communication), who documented increased heat loss and basal metabolic rate as possible causes of the runting.

Earlier work showed that *VHL* inactivation in the liver, either stochastically (in $VHL^{+/-}$ mice) or conditionally (in $VHL^{f/f}$ mice) in mice leads to hepatomegaly, steatosis, and blood vessel proliferation, including hemangioma-like lesions (Haase *et al*, 2001; Ma *et al*, 2003). A recent study showed that these lesions can be prevented by simultaneous inactivation of *ARNT*, but not by simultaneous inactivation of *HIF1α* (Rankin *et al*, 2005). This suggested that dysregulation of one or more ARNT partners is necessary, possibly in collaboration with other pVHL targets, for the development of these lesions.

Remarkably, we found that stabilization of HIF2α is sufficient to recapitulate the vascular liver lesions and hepatomegaly seen after pVHL loss and that dual stabilization of HIF1α and HIF2α is sufficient to induce to the other hepatic phenotypes linked to pVHL inactivation including macrovesicular steatosis. The apparent cooperation between HIF1α and HIF2α in the liver is consistent with earlier studies that concluded these two proteins are not wholly redundant. For example, it was shown earlier in other systems that the genes regulated by these two proteins, while overlapping, are non-identical (Hu *et al*, 2003; Raval *et al*, 2005; Wang *et al*, 2005), a result in keeping with our own microarray data. HIF2α, but not HIF1α, appears to act as an oncogene in pVHL-defective renal carcinomas, which also argues that the functions of HIF1α and HIF2α are not identical (Kondo *et al*, 2002, 2003; Maranchie *et al*, 2002; Zimmer *et al*, 2004; Raval *et al*, 2005).

Therefore, none of the many HIF-independent functions that have been ascribed to pVHL appear to play major roles in the skin and liver phenotypes observed so far after pVHL inactivation in keratinocytes and hepatocytes, respectively, with the caveat that the runting observed after hepatic pVHL inactivation was not recapitulated in the HIFdPA mice. This could reflect strain differences (although all phenotypes

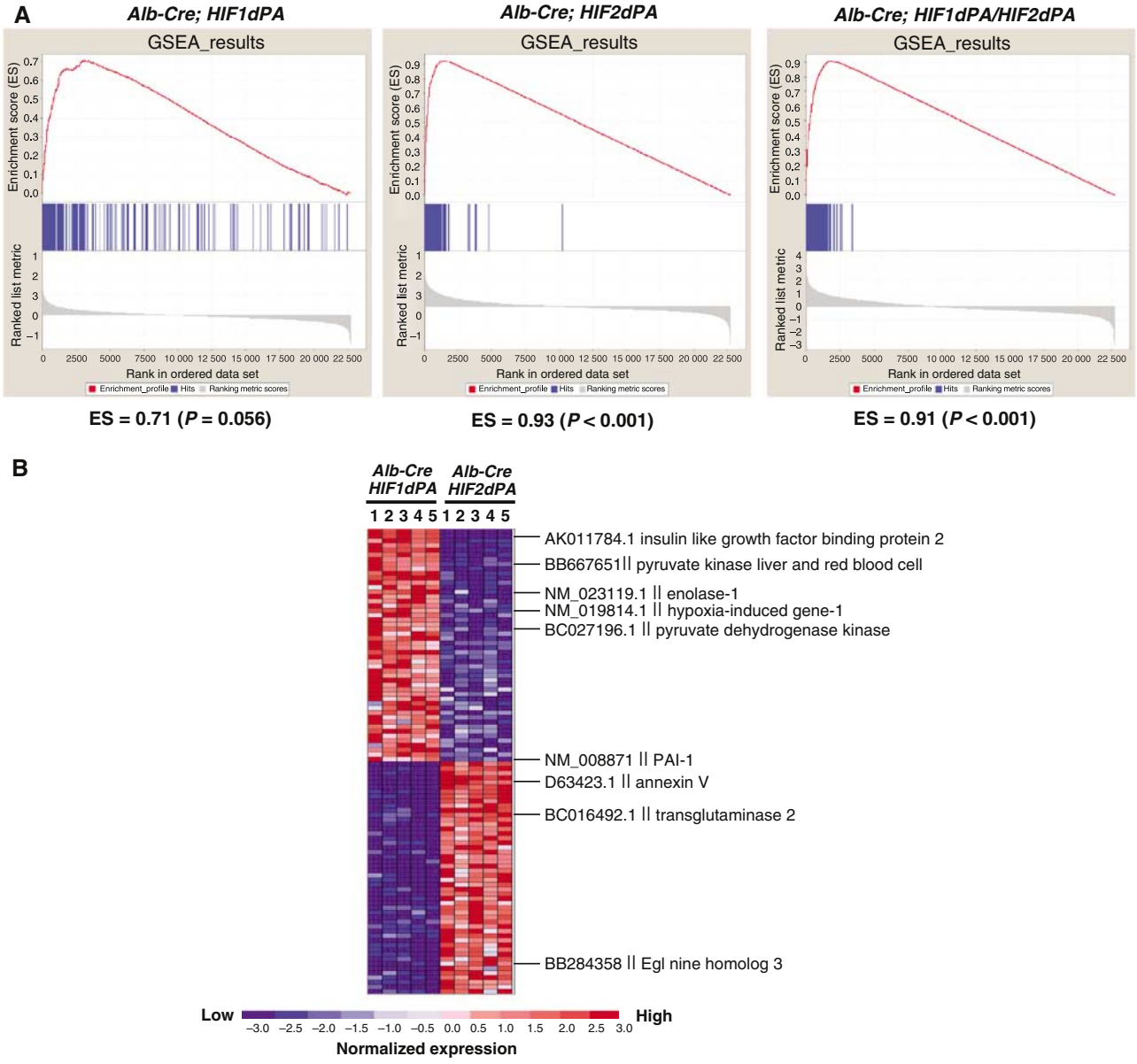

Figure 9 Gene-expression changes induced by pVHL loss or HIF activation. (**A**) Enrichment score as determined by GSEA comparing genes upregulated by pVHL loss in the liver to the expression profiles of livers from mice of the indicated genotype. Using the signal to noise ratio score, all genes on the array were ranked by their differential expression in samples from mice expressing constitutively active HIF1α (left), HIF2α (center), or both HIF1α and HIF2α (right) compared to samples from mice expressing the *Alb-Cre* control. GSEA was performed using a *VHL* signature comprised of the top 200 genes upregulated by *VHL* inactivation. The graphs in red show the enrichment scores. The vertical blue bars represent the position of each of the 200 genes in the *VHL* gene set in the ranked lists of the comparison groups. The graph in gray at the bottom shows the signal-to-noise score for each gene in the ranked list. (**B**) Top 100 genes differentially regulated by HIF1α or HIF2α. Each column represents a different sample and each row represents a different gene. The highest expression for each gene across samples is portrayed as red and the lowest expression in blue. The list of differentially regulated genes is included in the Supplementary data.

described were compared to littermate controls) or could reflect an HIF1/2-independent pVHL function. It also remains possible that HIF-independent pVHL functions are important in cell types and conditions that were not examined here. Nonetheless, our findings further validate HIF as a therapeutic target in pVHL-defective neoplasms, especially with respect to the angiogenesis that is characteristic of such lesions. In this regard, the mice described here might be useful for testing agents that inhibit HIF-dependent angiogenesis.

Neither pVHL inactivation nor HIFα stabilization has, to date, caused the emergence of solid tumors in mice. In particular, pVHL inactivation (or HIFα activation) in the mouse has not caused the development of clear cell renal carcinomas and pheochromocytomas observed in human VHL disease and the vascular lesions seen in the liver only loosely resemble hemangioblastomas. This might be because the correct cell has not yet been targeted in the mouse or because mice, in contrast to humans, are not permissive for the development of these tumors following pVHL inactivation (or HIFα activation). There are many examples of human cancer genes that, when mutated in the mouse, cause a different spectrum of tumors than observed in humans. This presumably reflects a variety of biological differences between mice and men that impact upon tissue tropism.

Nonetheless, the HIFdPA mice should be useful for asking whether HIF is sufficient to induce tumors in certain contexts and whether HIF, as suspected, can act as a progression factor in established tumors.

Materials and methods

Plasmids

pRosa26-PA and pBig-T vectors were gifts of Phillipe Soriano and Frank Constantini (Srinivas *et al*, 2001). The pBig-T plasmid contains two LoxP sites that flank a neomycin resistance gene, which is followed by a transcriptional Stop element. A multiple cloning site is present after the second LoxP site. The pRosa26-PA plasmid contains *ROSA26* genomic sequences into which a multiple cloning site containing *Asc*I and *Pac*I restriction sites has been inserted and a diphtheria toxin cassette 3′ of the *ROSA26* DNA for positive selection against nonhomologous recombinants.

pcDNA3.0-HA-HIF1α P402A;P564A and pcDNA3.0-HA-HIF2α P405A;P531A (Kondo *et al*, 2003) were cut with *Hin*dIII, blunt ended with T4 DNA polymerase (New England Biolabs), and recircularized to convert the *Hind*III site into an *Nhe*I restriction site. The HIFα cDNAs were then excised with *Nhe*I and *Not*I and ligated into pBigT that had been cut with these two enzymes to make pBigT-HA-HIF1α P402A;P564A and pBigT-HA-HIF2α P405A;P531A. The *Pac*I–*Asc*I fragments from these two plasmids were ligated into pRosa26-PA cut with the same enzymes to make the pRosa26-PA-HA-HIF1α P402A;P564A and pRosa26-PA-HA-HIF2α P405A;P531A targeting constructs.

Homologous recombination

The pRosa26-HA-HIF1α P402A;P564A and pRosa26-PA-HIF2α P405A;P531A targeting constructs were linearized with *Kpn*I and electroporated into TC1 ES cells derived from the 129 SVEV strain. G418 resistant HA-HIF1α P402A;P564A and HA-HIF2α P405A;P531A ES cell clones found to have undergone successful homologous recombination as detected by Southern blot analysis with a 5′ external *ROSA26* probe were microinjected into C57/BL6 blastocysts and implanted into pseudopregnant mothers to generate LSL-HIF1dPA and LSL-HIF2dPA chimeric mice that were backcrossed to Balb/C mice for three generations.

Mouse colony generation and maintenance

The *albumin-Cre* (*Alb-Cre*) C57/B6 mouse strain was purchased from Jackson Labs. The *keratin14-Cre* (*K14Cre*) FVB mouse strain was a generous gift from Pierre Chambon (IGBMC, University of Stasbourg) and the $VHL^{f/f}$ Balb/C mouse a generous gift from Volker Haase (University of Pennsylvania). Genomic DNA was isolated from mouse tails using a Puregene DNA Isolation Kit (Gentra Systems). Mice were genotyped by PCR (primers and conditions available upon request). All procedures involving mice were performed in accordance with the NIH guidelines for the use and care of live animals and were approved by the Dana-Farber Cancer Center IACUC.

Mouse embryo fibroblasts

MEFs were prepared using standard techniques and cultured in DMEM (Gibco) with 10% fetal bovine serum (Hyclone). Early passage MEFs was infected with adenoviral Cre (University of Iowa) at a MOI of 10 in the presence of 4 μg/ml of polybrene. MEFs were treated with MG132 (CalBiochem) for 6 h at a concentration of 30 μM.

Western blot analysis

Whole tissue or cell pellets were homogenized in 20 mM Tris (pH 7.5), 250 mM NaCl, 1 mM EDTA, 1 mM EGTA, and 1% Triton X-100 in the presence of a protease inhibitor cocktail (Roche). Whole-cell lysate (50 μg) or 100 μg of tissue homgenate, as determined by the Bradford method, was resolved by SDS–PAGE and transferred onto PVDF membranes. After blocking with Tris-buffered saline (TBS) with 4% non-fat milk the membranes were probed with anti-HA (HA-11) 1:1000 (Covance), anti-tubulin (DM1A) 1:2000 (Sigma), anti-HIF2α (BC100-480) 1:1000 (Novus), anti-HIF2α (NB100-122) 1:1000 (Novus), anti-HIF1α 1:5000 (Bethyl), and anti-HIF1α (NB100-449) 1:1000 (Novus), antibodies diluted in TBS with 4% bovine serum albumin. Bound antibody was detected with horse radish peroxidase-conjugated secondary antibody (Pierce) and SuperSignal West Pico chemiluminescent substrate (Pierce).

Histological studies

Tumor samples were fixed in 10% formalin overnight at room temperature, paraffin embedded, and stained with hematoxylin and eosin by standard methods. For immunohistochemisty, 5 μm sections were deparaffinized in xylene and rehydrated sequentially in ethanol. Antigen retrieval was performed by boiling in 10 mM sodium citrate (pH 6.0) for 30 min. Sections were stained with antibodies to CD31 (Pharmingen, 1:50), CD34 (Abcam, 1:500), and Ki67 (Vector Labs, 1:50). Oil red O (Sigma) staining was carried out on 10 μm frozen sections. The number of Ki67 positive cells was expressed as a percentage of positive staining cells over the total number of keratinocytes or hepatocytes per high powered field. Microvessel density was expressed as the number of microvessels per high powered field.

Evans blue vascular permeability assay

Mice (8–12 weeks old) were anesthetized (ketamine/xylazine) and administered 30 mg/kg Evans blue dye (Sigma) intravenously. Heavy mineral oil or mustard oil (Sigma; diluted to 5% in heavy mineral oil) was applied 10 and 20 min later. At 10 min after the last oil application, the mice were killed and the ears were dissected and weighed. Evans blue dye was extracted in 250 μl of 100% formamide overnight at 72°C. Extravasated dye was quantitated using a spectrophotometer (absorbance 610 nm) and corrected for background absorbance.

Hematologic studies

Whole blood was obtained by cardiac puncture of anesthetized mice just prior to euthanasia. Serum was prepared from whole blood using serum separator tubes and frozen at −80°C until use. Hematocrit levels and reticulocyte counts were measured using an Advia 120 hematology system on EDTA anticoagulated whole blood. Serum EPO was measured using an ELISA kit for mouse EPO (R&D Systems).

Statistical analysis

Statistical analyses were carried out with the variables in either their natural units or after log transformation. The data were analyzed using ANOVA followed by pairwise *t*-tests for comparisons of interest.

Gene expression analysis

Total RNA was isolated from mouse tissue using Trizol Reagent (Gibco) and then purified by the RNAeasy kit (Qiagen). Biotin labeled cRNA prepared from 15 μg of total RNA was fragmented and hybridized to mouse oligonucleotide arrays (Affymetrix, 430A 2.0 array). Preprocessing and normalization of the data were performed using Robust Multichip Averaging (Bolstad *et al*, 2003). Gene expression values less than a minimum threshold of 20 or a maximum threshold of 16 000 were set to 20 and 16 000, respectively. Genes with minimal variation across the data set were discarded (maximum/minimum <3 or maximum − minimum <100). Class neighbors were selected using GenePattern software (http://www.broad.mit.edu/cancer/software/genepattern) using the signal to noise metric (Golub *et al*, 1999). GSEA was performed as described (Subramanian *et al*, 2005).

Quantitative real-time PCR

Total RNA was isolated from MEFs using a QIAGEN RNeasy RNA isolation kit. Conversion into cDNA was performed using oligo-$dT_{(12-18)}$ (Invitrogen) and ImProm-II reverse transcriptase (Promega). PCR reactions using sequence specific primers and probes obtained from Applied Biosystems were performed in the ABI PRISM 7700 Sequence Detection System (Applied Biosystems). The PCR reactions were performed in duplicate for each cDNA, averaged, and normalized to endogenous ribosomal 18S reference transcripts.

Supplementary data

Supplementary data are available at *The EMBO Journal* Online (http://www.embojournal.org).

Acknowledgements

We thank Volker Haase and Pierre Chambon for mouse strains, Nabeel Bardeesy, Ron DePinho, Norman Sharpless, and James Horner for helpful advice, and members of the Kaelin Laboratory for useful discussions. This work was supported by grants from NIH to WYK and WGK and by a gift from the Murray Foundation. WGK is an HHMI Investigator.

References

Ang SO, Chen H, Hirota K, Gordeuk VR, Jelinek J, Guan Y, Liu E, Sergueeva AI, Miasnikova GY, Mole D, Maxwell PH, Stockton DW, Semenza GL, Prchal JT (2002) Disruption of oxygen homeostasis underlies congenital Chuvash polycythemia. *Nat Genet* **32:** 614–621

Aprelikova O, Chandramouli GV, Wood M, Vasselli JR, Riss J, Maranchie JK, Linehan WM, Barrett JC (2004) Regulation of HIF prolyl hydroxylases by hypoxia-inducible factors. *J Cell Biochem* **92:** 491–501

Bolstad BM, Irizarry RA, Astrand M, Speed TP (2003) A comparison of normalization methods for high density oligonucleotide array data based on variance and bias. *Bioinformatics* **19:** 185–193

Cockman ME, Masson N, Mole DR, Jaakkola P, Chang GW, Clifford SC, Maher ER, Pugh CW, Ratcliffe PJ, Maxwell PH (2000) Hypoxia inducible factor-alpha binding and ubiquitylation by the von Hippel-Lindau tumor suppressor protein. *J Biol Chem* **275:** 25733–25741

Compernolle V, Brusselmans K, Acker T, Hoet P, Tjwa M, Beck H, Plaisance S, Dor Y, Keshet E, Lupu F, Nemery B, Dewerchin M, Van Veldhoven P, Plate K, Moons L, Collen D, Carmeliet P (2002) Loss of HIF-2alpha and inhibition of VEGF impair fetal lung maturation, whereas treatment with VEGF prevents fatal respiratory distress in premature mice. *Nat Med* **8:** 702–710

Covello KL, Simon MC, Keith B (2005) Targeted replacement of hypoxia-inducible factor-1alpha by a hypoxia-inducible factor-2alpha knock-in allele promotes tumor growth. *Cancer Res* **65:** 2277–2286

Czyzyk-Krzeska MF, Meller J (2004) von Hippel-Lindau tumor suppressor: not only HIF's executioner. *Trends Mol Med* **10:** 146–149

Elson DA, Thurston G, Huang LE, Ginzinger DG, McDonald DM, Johnson RS, Arbeit JM (2001) Induction of hypervascularity without leakage or inflammation in transgenic mice overexpressing hypoxia-inducible factor-1alpha. *Genes Dev* **15:** 2520–2532

Gnarra JR, Ward JM, Porter FD, Wagner JR, Devor DE, Grinberg A, Emmert-Buck MR, Westphal H, Klausner RD, Linehan WM (1997) Defective placental vasculogenesis causes embryonic lethality in VHL-deficient mice. *Proc Natl Acad Sci USA* **94:** 9102–9107

Gnarra JR, Zhou S, Merrill MJ, Wagner JR, Krumm A, Papavassiliou E, Oldfield EH, Klausner RD, Linehan WM (1996) Post-transcriptional regulation of vascular endothelial growth factor mRNA by the product of the VHL tumor suppressor gene. *Proc Natl Acad Sci USA* **93:** 10589–10594

Golub TR, Slonim DK, Tamayo P, Huard C, Gaasenbeek M, Mesirov JP, Coller H, Loh ML, Downing JR, Caligiuri MA, Bloomfield CD, Lander ES (1999) Molecular classification of cancer: class discovery and class prediction by gene expression monitoring. *Science* **286:** 531–537

Gordeuk VR, Sergueeva AI, Miasnikova GY, Okhotin D, Voloshin Y, Choyke PL, Butman JA, Jedlickova K, Prchal JT, Polyakova LA (2004) Congenital disorder of oxygen sensing: association of the homozygous Chuvash polycythemia VHL mutation with thrombosis and vascular abnormalities but not tumors. *Blood* **103:** 3924–3932

Haase VH, Glickman JN, Socolovsky M, Jaenisch R (2001) Vascular tumors in livers with targeted inactivation of the von Hippel-Lindau tumor suppressor. *Proc Natl Acad Sci USA* **98:** 1583–1588

Hoffman MA, Ohh M, Yang H, Klco JM, Ivan M, Kaelin Jr WG (2001) von Hippel-Lindau protein mutants linked to type 2C VHL disease preserve the ability to downregulate HIF. *Hum Mol Genet* **10:** 1019–1027

Hu CJ, Wang LY, Chodosh LA, Keith B, Simon MC (2003) Differential roles of hypoxia-inducible factor 1alpha (HIF-1alpha) and HIF-2alpha in hypoxic gene regulation. *Mol Cell Biol* **23:** 9361–9374

Iliopoulos O, Levy AP, Jiang C, Kaelin Jr WG, Goldberg MA (1996) Negative regulation of hypoxia-inducible genes by the von Hippel-Lindau protein. *Proc Natl Acad Sci USA* **93:** 10595–10599

Indra AK, Li M, Brocard J, Warot X, Bornert JM, Gerard C, Messaddeq N, Chambon P, Metzger D (2000) Targeted somatic mutagenesis in mouse epidermis. *Horm Res* **54:** 296–300

Isaacs JS, Jung YJ, Mimnaugh EG, Martinez A, Cuttitta F, Neckers LM (2002) Hsp90 regulates a von Hippel Lindau-independent hypoxia-inducible factor-1 alpha-degradative pathway. *J Biol Chem* **277:** 29936–29944

Iyer NV, Kotch LE, Agani F, Leung SW, Laughner E, Wenger RH, Gassmann M, Gearhart JD, Lawler AM, Yu AY, Semenza GL (1998) Cellular and developmental control of O2 homeostasis by hypoxia-inducible factor 1 alpha. *Genes Dev* **12:** 149–162

Jackson EL, Willis N, Mercer K, Bronson RT, Crowley D, Montoya R, Jacks T, Tuveson DA (2001) Analysis of lung tumor initiation and progression using conditional expression of oncogenic K-ras. *Genes Dev* **15:** 3243–3248

Jiang Y, Zhang W, Kondo K, Klco JM, St Martin TB, Dufault MR, Madden SL, Kaelin Jr WG, Nacht M (2003) Gene expression profiling in a renal cell carcinoma cell line: dissecting VHL and hypoxia-dependent pathways. *Mol Cancer Res* **1:** 453–462

Kaelin Jr WG (2002) Molecular basis of the VHL hereditary cancer syndrome. *Nat Rev Cancer* **2:** 673–682

Kaelin Jr WG (2005) The von Hippel-Lindau protein, HIF hydroxylation, and oxygen sensing. *Biochem Biophys Res Commun* **338:** 627–638

Kim WY, Kaelin WG (2004) Role of VHL gene mutation in human cancer. *J Clin Oncol* **22:** 4991–5004

Kondo K, Kim WY, Lechpammer M, Kaelin Jr WG (2003) Inhibition of HIF2alpha is sufficient to suppress pVHL-defective tumor growth. *PLoS Biol* **1:** E83

Kondo K, Klco J, Nakamura E, Lechpammer M, Kaelin Jr WG (2002) Inhibition of HIF is necessary for tumor suppression by the von Hippel-Lindau protein. *Cancer Cell* **1:** 237–246

Larcher F, Murillas R, Bolontrade M, Conti CJ, Jorcano JL (1998) VEGF/VPF overexpression in skin of transgenic mice induces angiogenesis, vascular hyperpermeability and accelerated tumor development. *Oncogene* **17:** 303–311

Ma W, Tessarollo L, Hong SB, Baba M, Southon E, Back TC, Spence S, Lobe CG, Sharma N, Maher GW, Pack S, Vortmeyer AO, Guo C, Zbar B, Schmidt LS (2003) Hepatic vascular tumors, angiectasis in multiple organs, and impaired spermatogenesis in mice with conditional inactivation of the VHL gene. *Cancer Res* **63:** 5320–5328

Mandriota SJ, Turner KJ, Davies DR, Murray PG, Morgan NV, Sowter HM, Wykoff CC, Maher ER, Harris AL, Ratcliffe PJ, Maxwell PH (2002) HIF activation identifies early lesions in VHL kidneys: evidence for site-specific tumor suppressor function in the nephron. *Cancer Cell* **1:** 459–468

Mao X, Fujiwara Y, Chapdelaine A, Yang H, Orkin SH (2001) Activation of EGFP expression by Cre-mediated excision in a new ROSA26 reporter mouse strain. *Blood* **97:** 324–326

Maranchie JK, Vasselli JR, Riss J, Bonifacino JS, Linehan WM, Klausner RD (2002) The contribution of VHL substrate binding and HIF1-alpha to the phenotype of VHL loss in renal cell carcinoma. *Cancer Cell* **1:** 247–255

Masson N, Willam C, Maxwell PH, Pugh CW, Ratcliffe PJ (2001) Independent function of two destruction domains in hypoxia-inducible factor-alpha chains activated by prolyl hydroxylation. *EMBO J* **20:** 5197–5206

Maxwell PH, Wiesener MS, Chang GW, Clifford SC, Vaux EC, Cockman ME, Wykoff CC, Pugh CW, Maher ER, Ratcliffe PJ (1999) The tumour suppressor protein VHL targets hypoxia-inducible factors for oxygen-dependent proteolysis. *Nature* **399:** 271–275

Pastore YD, Jelinek J, Ang S, Guan Y, Liu E, Jedlickova K, Krishnamurti L, Prchal JT (2003) Mutations in the VHL gene in sporadic apparently congenital polycythemia. *Blood* **101:** 1591–1595

Peng J, Zhang L, Drysdale L, Fong GH (2000) The transcription factor EPAS-1/hypoxia-inducible factor 2alpha plays an important role in vascular remodeling. *Proc Natl Acad Sci USA* **97:** 8386–8391

Postic C, Shiota M, Niswender KD, Jetton TL, Chen Y, Moates JM, Shelton KD, Lindner J, Cherrington AD, Magnuson MA (1999) Dual roles for glucokinase in glucose homeostasis as determined by liver and pancreatic beta cell-specific gene knock-outs using Cre recombinase. *J Biol Chem* **274:** 305–315

Rankin EB, Higgins DF, Walisser JA, Johnson RS, Bradfield CA, Haase VH (2005) Inactivation of the arylhydrocarbon receptor nuclear translocator (Arnt) suppresses von Hippel-Lindau disease-associated vascular tumors in mice. *Mol Cell Biol* **25:** 3163–3172

Raval RR, Lau KW, Tran MG, Sowter HM, Mandriota SJ, Li JL, Pugh CW, Maxwell PH, Harris AL, Ratcliffe PJ (2005) Contrasting properties of hypoxia-inducible factor 1 (HIF-1) and HIF-2 in von Hippel-Lindau-associated renal cell carcinoma. *Mol Cell Biol* **25:** 5675–5686

Ravi R, Mookerjee B, Bhujwalla ZM, Sutter CH, Artemov D, Zeng Q, Dillehay LE, Madan A, Semenza GL, Bedi A (2000) Regulation of tumor angiogenesis by p53-induced degradation of hypoxia-inducible factor 1alpha. *Genes Dev* **14:** 34–44

Schofield CJ, Ratcliffe PJ (2004) Oxygen sensing by HIF hydroxylases. *Nat Rev Mol Cell Biol* **5:** 343–354

Schofield CJ, Ratcliffe PJ (2005) Signalling hypoxia by HIF hydroxylases. *Biochem Biophys Res Commun* **338:** 617–626

Semenza GL (2003) Targeting HIF-1 for cancer therapy. *Nat Rev Cancer* **3:** 721–732

Siemeister G, Weindel K, Mohrs K, Barleon B, Martiny-Baron G, Marme D (1996) Reversion of deregulated expression of vascular endothelial growth factor in human renal carcinoma cells by von Hippel-Lindau tumor suppressor protein. *Cancer Res* **56:** 2299–2301

Soriano P (1999) Generalized lacZ expression with the ROSA26 Cre reporter strain. *Nat Genet* **21:** 70–71

Srinivas S, Watanabe T, Lin CS, William CM, Tanabe Y, Jessell TM, Costantini F (2001) Cre reporter strains produced by targeted insertion of EYFP and ECFP into the ROSA26 locus. *BMC Dev Biol* **1:** 4

Stratmann R, Krieg M, Haas R, Plate KH (1997) Putative control of angiogenesis in hemangioblastomas by the von Hippel-Lindau tumor suppressor gene. *J Neuropathol Exp Neurol* **56:** 1242–1252

Subramanian A, Tamayo P, Mootha VK, Mukherjee S, Ebert BL, Gillette MA, Paulovich A, Pomeroy S, Golub TR, Lander ES, Mesirov J (2005) Gene set enrichment analysis: a knowledge-based approach for interpreting genome-wide expression profiles. *Proc Natl Acad Sci USA* **102:** 15545–15550

Thurston G, Suri C, Smith K, McClain J, Sato TN, Yancopoulos GD, McDonald DM (1999) Leakage-resistant blood vessels in mice transgenically overexpressing angiopoietin-1. *Science* **286:** 2511–2514

Tian H, Hammer RE, Matsumoto AM, Russell DW, McKnight SL (1998) The hypoxia-responsive transcription factor EPAS1 is essential for catecholamine homeostasis and protection against heart failure during embryonic development. *Genes Dev* **12:** 3320–3324

Vincent KA, Shyu KG, Luo Y, Magner M, Tio RA, Jiang C, Goldberg MA, Akita GY, Gregory RJ, Isner JM (2000) Angiogenesis is induced in a rabbit model of hindlimb ischemia by naked DNA encoding an HIF-1alpha/VP16 hybrid transcription factor. *Circulation* **102:** 2255–2261

Wang V, Davis DA, Haque M, Huang LE, Yarchoan R (2005) Differential gene up-regulation by hypoxia-inducible factor-1alpha and hypoxia-inducible factor-2alpha in HEK293T cells. *Cancer Res* **65:** 3299–3306

Wykoff CC, Pugh CW, Maxwell PH, Harris AL, Ratcliffe PJ (2000) Identification of novel hypoxia dependent and independent target genes of the von Hippel-Lindau (VHL) tumour suppressor by mRNA differential expression profiling. *Oncogene* **19:** 6297–6305

Wykoff CC, Sotiriou C, Cockman ME, Ratcliffe PJ, Maxwell P, Liu E, Harris AL (2004) Gene array of VHL mutation and hypoxia shows novel hypoxia-induced genes and that cyclin D1 is a VHL target gene. *Br J Cancer* **90:** 1235–1243

Zambrowicz BP, Imamoto A, Fiering S, Herzenberg LA, Kerr WG, Soriano P (1997) Disruption of overlapping transcripts in the ROSA beta geo 26 gene trap strain leads to widespread expression of beta-galactosidase in mouse embryos and hematopoietic cells. *Proc Natl Acad Sci USA* **94:** 3789–3794

Zatyka M, da Silva NF, Clifford SC, Morris MR, Wiesener MS, Eckardt KU, Houlston RS, Richards FM, Latif F, Maher ER (2002) Identification of cyclin D1 and other novel targets for the von Hippel-Lindau tumor suppressor gene by expression array analysis and investigation of cyclin D1 genotype as a modifier in von Hippel-Lindau disease. *Cancer Res* **62:** 3803–3811

Zimmer M, Doucette D, Siddiqui N, Iliopoulos O (2004) Inhibition of hypoxia-inducible factor is sufficient for growth suppression of VHL−/− tumors. *Mol Cancer Res* **2:** 89–95

